Minimizing the Water Resonance in Biological NMR: Characterization and Suppression of Intermolecular Dipolar Interactions by Multiple-Axis Gradients[⊥]

Debra L. Mattiello,[†] Warren S. Warren,[‡] Luciano Mueller,[ϕ] and Bennett T. Farmer II*,[ϕ]

Contribution from the Department of Research & Development, NMR Instrument Division, Varian Associates, Palo Alto, California 94304, Department of Chemistry, Princeton University, Princeton, New Jersey 08543, and Pharmaceutical Research Institute, Bristol-Myers Squibb, P.O. Box 4000, Princeton, New Jersey 08543-4000

Received September 18, 1995[⊗]

Abstract: Anomalous crosspeaks and additional resonances in the indirectly detected dimension have been previously observed in a number of 2D NMR experiments applied to samples having at least one concentrated species. These unexpected peaks exhibit all the characteristics of intermolecular multiple-quantum coherences. Since these coherences are possible within the concentrated species alone, their creation and subsequent detection may be one of the causes for poor water suppression in a variety of biomolecular NMR experiments, e.g., the conventional MQ-filtered- (MQF) and MQ-COSY experiments applied to proteins/peptides in 90% water. In this report, we experimentally characterize the creation/observation of intermolecular water−water MQ coherences using variable-angle pulsed field gradients. We show that the existing theoretical picture is consistent with all of our experimental observations, thereby validating the predictive power of the intuition gained from this picture. We also provide an increased understanding of the effect that variable-angle gradients can have on the intensity of observable magnetization arising from these intermolecular MQ coherences. Finally, we establish a basis on which one may reasonably speculate concerning the impact of these coherences on water suppression within the repertoire of gradient-enhanced heteronuclear experiments that are currently being applied to $^{13}C/^{15}N$ isotopically labeled proteins in 90% water.

Introduction

Anomalous crosspeaks and additional resonances in the indirectly detected dimension have been previously observed in a number of 2D NMR experiments applied to samples having at least one concentrated species,[1−10] e.g., a protein in 90% water. These unexpected peaks exhibit all the characteristics of intermolecular multiple-quantum (MQ) coherences,[1,2] the existence of which, however, is impossible under the traditional theoretical framework of high-field NMR. Previous studies have focused on intermolecular coherences either between a concentrated and a dilute species[2] or between two concentrated species[1] in order to provide a better understanding of their underlying physical basis. Such coherences, however, are also possible within a single concentrated species,[1,5] e.g., 90% water, in analogy to what has already been observed for the phenomena of multiple spin echoes (MSEs).[11,12] Intermolecular water−water MQ coherences may therefore be one of the major causes for poor water suppression[13] in the conventional MQ-filtered- (MQF) and MQ-COSY experiments[14,15] applied to proteins/peptides in 90% water.

The basis for the intermolecular MQ coherences has been recently described using a general density-matrix framework.[2] To account for these coherences, four additional factors have been introduced into the conventional density-matrix treatment of NMR: (1) retention of higher order terms in the equilibrium density matrix (σ^o); (2) recognition of a cutoff distance (r_{cutoff}) beyond which diffusional averaging cannot eliminate the first-order dipolar coupling; (3) incomplete macroscopic averaging of intermolecular first-order dipolar coupling due to gradient-induced spin asymmetry; and (4) macroscopic dipolar refocusing of intermolecular single-quantum coherence to observable magnetization during the acquisition period. The third factor speaks to the fact that the macroscopic cancellation of any first-order dipolar effect in solution requires spherical symmetry in the total spin environment. If these additions to the conventional density-matrix picture are accepted, explicit predictions can be made about both the general magnitude of these intermolecular

* To whom correspondence should be addressed.
[†] Varian Associates.
[‡] Princeton University.
[ϕ] Bristol-Myers Squibb.

[⊥] Keywords: intermolecular multiple-quantum coherences; multiple-axis gradients; magic-angle gradients; nQF-COSY; water suppression; NMR.
[⊗] Abstract published in *Advance ACS Abstracts,* March 1, 1996.

(1) He, Q.; Richter, W.; Vathyam, S.; Warren, W. S. *J. Chem. Phys.* **1993**, *98*, 6779−6800.
(2) Warren, W. S.; Richter, W.; Andreotti, A. H.; Farmer II, B. T. *Science* **1993**, *262*, 2005−2009.
(3) Richter, W.; Lee, S.; Warren, W. S.; He, Q. *Science* **1995**, *267*, 654−657.
(4) McCoy, M.; Warren, W. S. *J. Chem. Phys.* **1990**, *96*, 858−859.
(5) Warren, W. S.; He, Q.; McCoy, M.; Spano, F. C. *J. Chem. Phys.* **1992**, *96*, 1659−1661.
(6) Mattiello, D. L.; Montelione, G. T.; Mueller, L.; Warren, W. S.; Farmer II, B. T. Presented at the *Experimental NMR Conference*; Boston, MA, 1995.
(7) Zilm, K. Presented at the *American Physical Society Meeting*; Pittsburgh, PA, 1994.
(8) Bowden, C. J.; Heseltine, T.; Prandolini, M. J. *Chem. Phys. Lett.* **1995**, *233*, 639−641.
(9) Jeener, J.; Vlassenbroek, A.; Broekaert, P. *J. Magn. Reson. Ser. A* Submitted for publication.
(10) Levitt, M. *Concepts in Magnetic Resonance* **1996**, *8*, 77−103.
(11) Körber, H.; Dormann, E.; Eska, G. *J. Magn. Reson.* **1991**, *93*, 589−595.
(12) Bowtell, R.; Bowley, R. M.; Glover, P. *J. Magn. Reson.* **1990**, *88*, 643−651.
(13) van Zijl, P. C. M.; Johnson, M. O.; Mori, S.; Hurd, R. E. *J. Magn. Reson. Ser. A* **1995**, *113*, 265−270.
(14) Hurd, R. E. *J. Magn. Reson.* **1990**, *87*, 422−428.
(15) Davis, A. L.; Laue, E. D.; Keeler, J.; Moskau, D.; Lohman, J. *J. Magn. Reson.* **1991**, *94*, 637−644.

0002-7863/96/1518-3253$12.00/0 © 1996 American Chemical Society

multiple-quantum signals and the effects of gradient direction on their absolute intensities.

In this paper, we experimentally characterize the creation/observation of intermolecular water−water MQ coherences. We show that the theoretical picture in ref 2 is consistent with all of our experimental observations, thereby validating the predictive power of the intuition gained from this picture. We also provide an increased understanding of the effect that variable-angle gradients can have on the intensity of observable magnetization arising from these intermolecular MQ coherences. Finally, we establish a basis on which one may reasonably speculate concerning the impact of these coherences on water suppression within the repertoire of gradient-enhanced heteronuclear experiments that are currently being applied to $^{13}C/^{15}N$ isotopically labeled proteins in 90% water.

Dipolar Refocusing

The theoretical treatment in ref 2 predicts that the dipolar refocusing of an intermolecular two-quantum (2Q) coherence depends on $P_2(\cos\theta)$ where θ is the angle between the applied gradient vector and the axis of the static magnetic field. Suppression of this dipolar refocusing with a magic-angle gradient ($\theta = 54.7°$, $P_2(\cos\theta) = 0$) has previously been verified experimentally for the CRAZED sequence[16] (a COSY sequence which incorporates a 2Q filter[1,2]). A $P_2(\cos\theta)$ dependence was originally observed for the relative amplitude of the second stimulated echo in pure water following a $90°_x-\tau-90°_x$ sequence.[12] Within the density-matrix picture, we ascribe this echo to the dipolar refocusing of intermolecular single-quantum coherence between two water molecules. A $P_2(\cos\theta)$ dependence has also been recently demonstrated for the intensity of the residual water magnetization in the gradient-enhanced (GE) 2QF-COSY.[13] In the course of these investigations, we have reconfirmed the θ profile for dipolar refocusing of intermolecular 2Q coherence[6] and have also characterized the dipolar refocusing of even higher-order coherences.

Figure 1 depicts the GE MQF-COSY experiment used to characterize the effect of variable-angle gradients on the intensity of residual water magnetization. It is an adaptation of a previously published GE MQF-COSY experiment.[14,15] With this sequence, θ is the angle in spherical coordinates that describes the gradient direction in the *xz*-plane and is defined by the relation $\tan\theta = |G_x|/|G_z|$. $|G_x|$ and $|G_z|$ represent the magnitudes of the linear variation along *x* and *z*, respectively, for the *z*-component of the B_0 magnetic flux density. Similarly, ϕ is the angle in spherical coordinates that describes the gradient direction in the *xy*-plane and is defined by the relation $\tan\phi = |G_y|/|G_x|$. One can generalize the θ dependence of intermolecular *n*Q-derived signal by a simple extension of the original density-matrix analysis.[2]

Consider that the final 90_x pulse in Figure 1 converts the selected *n*Q coherence into *n*-spin, single-quantum coherence involving multiple water molecules, represented as

$$I_{xi}\prod_{k=1}^{n-1} I_{zk}$$

in the Cartesian-coordinate spin-operator formalism.[17] $n - 1$ dipolar couplings will be required during t_2 to refocus this *n*-spin single-quantum coherence to observable magnetization. Because each first-order coupling between pairs of spins can be treated independently, eq 7 in ref 2 can be modified to treat $n - 1$ dipolar couplings as follows:

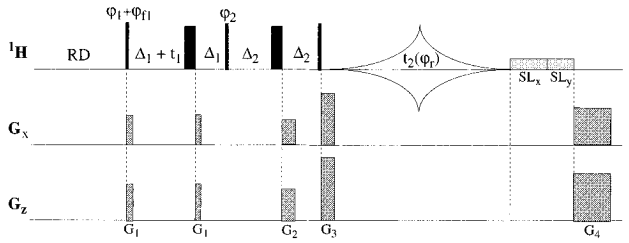

Figure 1. Gradient-enhanced nQF-COSY experiment with multiple-axis gradient capability. 90° RF pulses are represented by wide lines and 180° pulses, by black rectangles. RD is the relaxation delay. The recycle time, T_{RC}, is equal to (RD + t_2) where t_2 is the total acquisition time along the directly acquired dimension. SL_x and SL_y indicate proton RF purge pulses[29] with phases *x* and *y*, respectively. Δ_1 and Δ_2 are gradient recovery delays and are typically set to 0.4 and 1.1 ms, respectively. G_z and G_x are defined as $dB_0(z)/dz$ and $dB_0(z)/dx$, respectively, and denote the linear variation along *z* and *x*, respectively, of the *z*-component of the magnetic flux density. The angle θ is defined by the relation $\tan\theta = |G_x|/|G_z|$, and the angle ϕ is defined by the relation $\tan\phi = |G_y|/|G_x|$. All gradient pulses within a given experiment have the same (θ, ϕ) angles. Gradients G_1 and G_4 are typically set to (7.9 G/cm, 0.3 ms) and (14.8 G/cm, 10 ms), respectively, in magnitude and duration. We have also introduced a small but practical modification to an existing approach for eliminating the 180° refocusing pulse prior to the t_2 acquisition period,[15] which is normally required to obtain phase-sensitive data in F_2. It may be quite difficult to synchronize data collection with other hardware events, e.g., gradient and RF pulses, when the latter occur during only part of the acquisition period. Instead of starting data acquisition immediately after the third 90° pulse, regardless of the state of the receiver, we have elected to start the t_2 data collection at a time after the final 90° pulse corresponding to some multiple *j* of the spectral width. The minimum value for this time would be that necessary to accommodate both the G_3 gradient pulse and its associated recovery delay. Prior to conventional processing, the FID data is right-shifted *j* points and padded at the front with *j* zeroes as previously described.[15]

$$S_n \propto (t_2^{\,n-1})\prod_{k=1}^{n-1}\left|\sum_{j=1}^{N} D_{1j}\cos(\gamma G s_j T)\right| \qquad (1)$$

where S_n is the time-domain intensity of the intermolecular *n*Q-derived signal at a particular time t_2 in the acquisition dimension; D_{1j} is the dipolar coupling between spins 1 and *j*; *G* is the strength of the gradient pulse directed along an axis defined by the vector **s**; and $s_j = \mathbf{r}_j\cdot\mathbf{s}$ with $\mathbf{r}_j$ representing the vector from the origin to spin *j*. The sum in eq 1 can be replaced by an integral over the sample volume, which, for $\gamma G r_{cutoff} T \ll 1$, evaluates as proportional to

$$[3(\mathbf{s}\cdot\mathbf{z})^2 - 1]/2 \equiv P_2(\cos\theta) \qquad (2)$$

where $\cos\theta = \mathbf{s}\cdot\mathbf{z}$. Using the result in eq 2, one can simplify eq 1 to be

$$S_n \propto (t_2^{\,n-1})\prod_{k=1}^{n-1}|P_2(\cos\theta)| \qquad (3a)$$

$$= (t_2^{\,n-1})|[P_2(\cos\theta)]^{n-1}| \qquad (3b)$$

S_n is related by Fourier transformation to I_n, the frequency-domain intensity of the intermolecular *n*Q-derived signal. Because any θ or ϕ dependence is invariant to Fourier transformation, eq 3b predicts that I_n scales with $[P_2(\cos\theta)]^{n-1}$ and that I_n is independent of ϕ.

We have experimentally verified these two predictions of eq 3b. Figure 2 (parts A and B) presents 1D data from a GE 3QF-

(16) Richter, W.; Warren, W. S. *Encycl. Magn. Reson.* **1996**, in press.
(17) Sørensen, O. W.; Eich, G. W.; Levitt, M. H.; Bodenhausen, G.; Ernst, R. R. *Prog. Nucl. Magn. Reson. Spectrosc.* **1983**, *16*, 163−192.

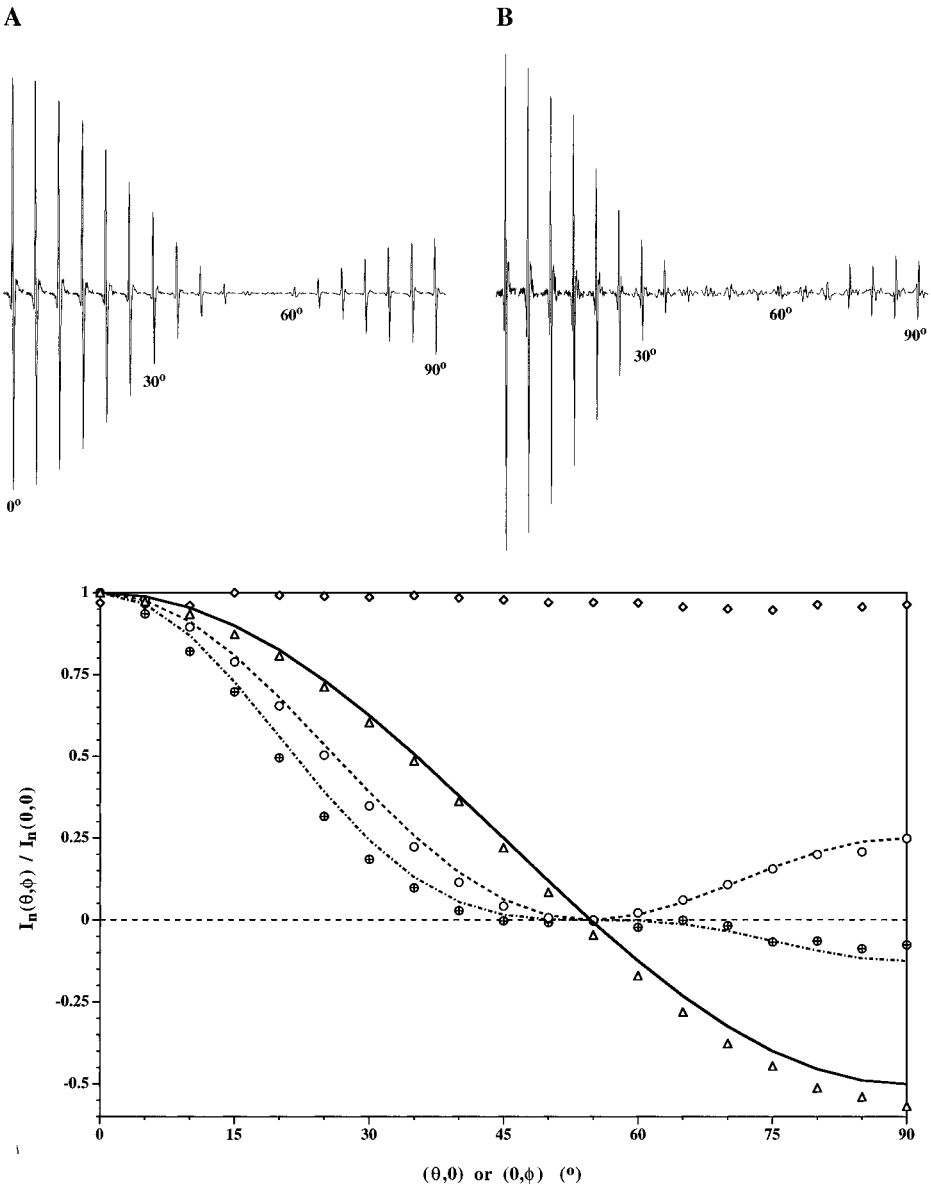

Figure 2. (A) The antiphase signal from residual water following a 3Q gradient filter is displayed as a function of θ with ϕ fixed at 0° for sgn(G_2/G_3) = 1. The intensity of the antiphase signal, $I_3(\theta, \phi)$, is defined as ($h_{df} - h_{uf}$)/2 where h_{df} and h_{uf} are the maximum heights of the downfield and upfield peaks, respectively, in the antiphase resonance. The baseline defines the zero level. (B) The antiphase signal from residual water following a 4Q gradient filter is displayed as a function of θ with ϕ fixed at 0° for sgn(G_2/G_3) = 1. (C) Experimental $I_n(\theta, 0)/I_n(0, 0)$ ratios are plotted as a function of θ for $n = 2$ (△), 3 (○), and 4 (⊕). Calculated $[P_2(\cos\theta)]^{n-1}$ curves are drawn for $n = 2$ (—), 3 (— —), and 4 (— · — ·). Experimental $I_2(0, \phi)/I_2(0, 0)$ ratios are plotted as a function of ϕ (black, ◇). The sample was 2 mM unlabeled BPTI in 90% water. The pulse sequence and parameters described in Figure 1 were used with sgn(G_2/G_3) = 1 for data acquisition. The data were collected at 30.0 °C on a Varian UnityPlus 500 using a $^1H/^{13}C/^{15}N$ triple-resonance probe equipped with a self-shielded triple-axis gradient coil. The relative G_z and G_x gradient strengths were calibrated in the following manner. Briefly, the gradient amplifier DAC value for the *x* axis, DAC_{Gx}, was set to 13058 and that for the *z*-axis, DAC_{Gz}, to 9246, corresponding to a gradient pulse theoretically at (θ, ϕ) = (54.7°, 0°). DAC_{Gz} was then scaled by the *x*-gradient strength relative to the z gradient strength as measured by a gradient profile experiment. The calibration was then refined as previously described.[13] With $\theta \sim 54.7°$, DAC_{Gz} was adjusted to DAC_{Gz}^{final} in order to achieve a null in the residual water signal following a 2Q gradient filter. The calibration constant between the *z*-axis gradient and the *x*-axis gradient, which is analogous to the ratio $|G_z|/|G_x|$ for a uniform DAC value, is then given by ($DAC_{Gz}^{final}/DAC_{Gx}$)*tan(54.7°).

and 4QF-COSY, respectively, on 2 mM BPTI in 90% water. No phase cycling was utilized in collecting these data; and $\varphi_{f1} = \varphi_1 = \varphi_2 = x$. θ was varied from 0° to 90° in steps of 5°. These sets of spectra illustrate the line shape of the residual water resonance and demonstrate the effect of θ on both the intensity and absolute phase of this resonance as a function of the coherence order of the filter. Figure 2C presents both experimental and calculated phase-sensitive θ profiles of residual water magnetization arising from intermolecular 2Q, 3Q, and 4Q coherences during the two Δ_2 periods in the pulse sequence. The experimental phase-sensitive ϕ profile of residual water magnetization arising from intermolecular 2Q coherence is also graphed in Figure 2C. Phase-sensitive peak intensities, $I_n(\theta, \phi)$ are defined as ($h_{df} - h_{uf}$)/2 where h_{df} and h_{uf} are the maximum heights of the downfield and upfield peaks, respectively, in the antiphase resonance of the *n*Q-filtered residual water. For reference, the baseline defines the zero level. All experimental $I_n(\theta, \phi)$ values have been normalized to the peak intensity obtained for $\theta = 0°$ and $\phi = 0°$, which corresponds to $I_n(0, 0)$.

Four observations are readily made concerning the data presented in Figure 2. Firstly, the residual water resonance in

Figure 2 (parts A and B) exhibits an antiphase line shape. This is consistent with the water magnetization being rendered observable during the detection period by a refocusing mechanism, e.g., dipolar coupling. Secondly, the relative phase of the resonance in Figure 2A, which arises from 3Q-filtered residual water, does not change as θ is increased from 0° to 90°. Such behavior is expected for all odd coherence-order filters. In contrast, an equivalent set of spectra from the GE 4QF-COSY (Figure 2B) exhibits a phase inversion as θ is increased. A phase inversion is also observed in the GE 2QF-COSY set of spectra (Figure 8 in supporting information). In both the 2Q and 4Q cases, this phase inversion occurs around $\theta \sim 55°$ and is expected for all even coherence-order filters. Thirdly, a comparison of each set of experimental $I_n(\theta, 0)/I_n(0, 0)$ ratios with its respective $[P_2(\cos\theta)]^{n-1}$ curve in Figure 2C reveals a strong correlation. In addition, the experimental $I_2(0, \phi)/I_2(0, 0)$ ratio varies minimally with ϕ in Figure 2C. Both the θ dependence and the ϕ dependence of I_n predicted by eq 3b have therefore been validated by experiment. Finally, a single-axis transverse gradient is noted to be 2^{n-1} more effective than its axial counterpart in suppressing residual water magnetization arising from intermolecular nQ coherences that exist during the two Δ_2 periods.

Higher Order Terms in σ^o

Retention of higher order terms in the equilibrium density matrix (σ^o) is a key factor in the density-matrix theory that explains the intermolecular water−water MQ coherences.[2] From previous control experiments, we have observed that the intermolecular solute−water 2Q correlations exhibit the same relative phase whether the first pulse in the CRAZED pulse sequence produces a 90° or a 270° spin rotation. This can only occur if the correlations arise from initial states represented by products of an even number of I_z terms, e.g., $I_{zi}I_{zj}$. States with an odd number of I_z terms, e.g., I_{zi} and $I_{zi}I_{zj}I_{zk}$, must show an inversion of phase in going from a 90° to a 270° tip angle for the initial pulse. Furthermore, the long relaxation delay (25 s) used in those experiments has precluded any relaxation-based memory effects between transients.

To address more thoroughly the relationship between higher order terms in σ^o and intermolecular nQ coherences, we have collected a more quantitative set of data in this study. Figure 3 presents data on intermolecular 2Q- and 3Q-derived residual water magnetization acquired using the pulse sequence of Figure 1 under the following conditions: θ is fixed at 0° (axial gradient); the ^{1}H carrier is placed 500 Hz downfield of the water resonance; and the t_1 evolution time is incremented from 0 to 10 ms in steps of 100 μs. If $t_1 = 0$, terms in the Taylor series expansion of σ^o such as

$$I_{z1}\prod_{k=2}^{n} I_{zk} \tag{4a}$$

are rotated to

$$(-1)^n I_{z1}\prod_{k=2}^{n} I_{zk} \tag{4b}$$

by the second 90_x pulse. No intermolecular water−water nQ coherence is therefore present during the two Δ_2 periods to be selected by the G_1 gradient. If $t_1 = 1/[4*(\nu_{water} - \nu_{carrier})]$, the first three pulses in Figure 1 transform the states described by eq 4a into

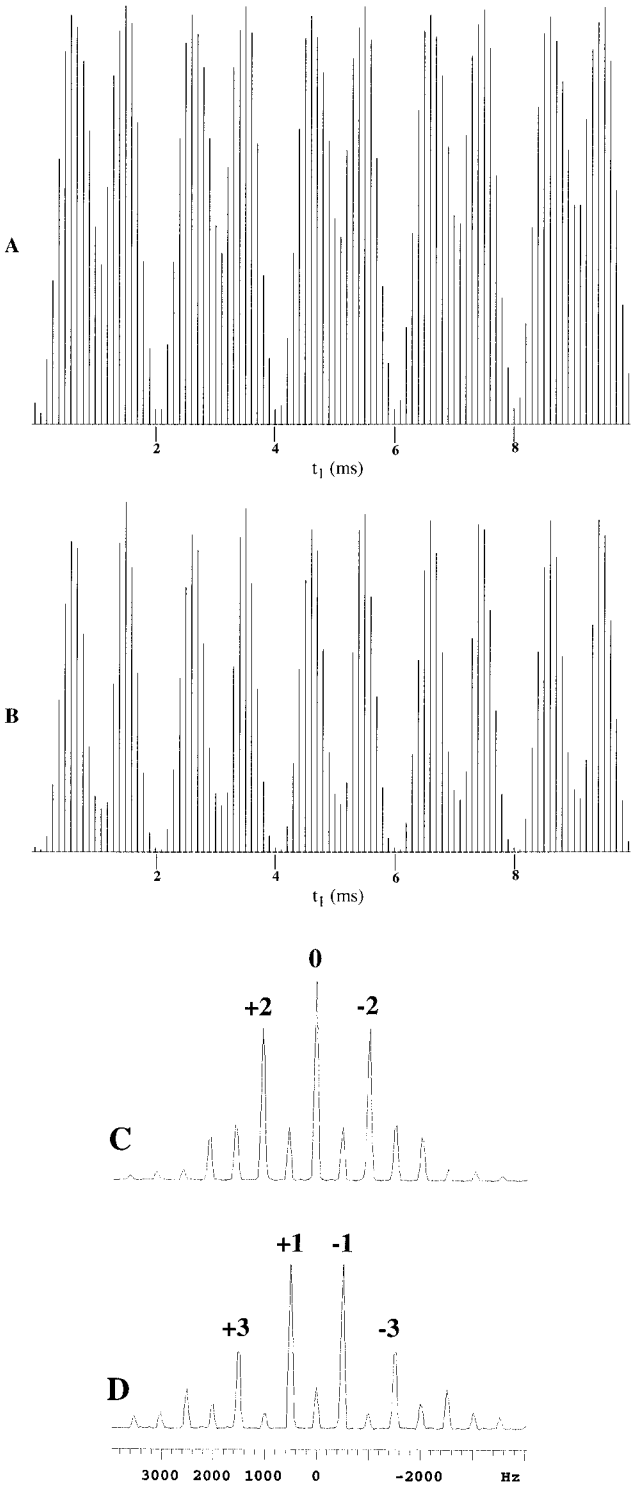

Figure 3. The t_1 time-domain profile ($n = 2, 3$) and the F_1 frequency-domain profiles ($n = 2, 3$) of the residual water signal following an nQ gradient filter with $\theta = 0°$ and $\phi = 90°$ are shown. The pulse sequence in Figure 1 was used. The ^{1}H carrier was placed 500 Hz upfield of the water resonance ($\Delta\Omega/2\pi = 500$ Hz), and a relaxation delay of 20 s (RD in Figure 1) was used. Important resonances are labeled with their corresponding $\Delta\Omega$ harmonic value. The residual water signal intensity is displayed in absolute value mode. t_1 ranges from 0 to 10 ms in steps of 100 μs. The data were collected at 30.0 °C on a Varian UnityPlus 500 using a ^{1}H/^{13}C/^{15}N triple-resonance probe equipped with a self-shielded triple-axis gradient coil: (A) 2Q t_1 profile, (B) 3Q t_1 profile, (C) 2Q F_1 profile, (D) 3Q F_1 profile.

$$I_{x1}\prod_{k=2}^{n} I_{xk} \tag{5}$$

just prior to the first Δ_2 period, which gives rise to the maximum intensity of intermolecular *n*Q coherences during the Δ_2 periods. For example, $I_{x1}I_{x2}$ can be decomposed into the following ZQ and DQ terms:

$$\text{ZQ:}\quad (I_1^+I_2^- + I_1^-I_2^+)/4 \tag{6a}$$

$$\text{DQ:}\quad (I_1^+I_2^+ + I_1^-I_2^-)/4 \tag{6b}$$

The signal intensity of an *n*-spin, *n*Q term, $S_n(t_1)$, depends therefore on t_1 and is described analytically by eq 7

$$S_n(t_1) = \sin^n[\Omega_{\text{water}}t_1] \tag{7}$$

where $\Omega_{\text{water}} = 2\pi\ (\nu_{\text{water}} - \nu_{\text{carrier}})$.

Peak intensities of residual water from the 2Q- and 3Q-filtered data acquired in this manner are displayed as a function of t_1 in Figure 3 (parts A and B, respectively). Figure 3 (parts C and D) presents the experimental F_1 frequency profiles for intermolecular 2Q- and 3Q-derived residual water magnetization, respectively, obtained by Fourier transformation of the t_1 interferogram taken at the center of the water resonance in F_2. The relationship between these experimental F_1 frequency profiles and the theoretical quantity $S_n(t_1)$ defined in eq 7 is more easily seen by recasting eq 7 in a Fourier series specifically for the $n = 2$ (2Q) and $n = 3$ (3Q) cases:

$$S_2(t_1) = 1 - \cos(2\Omega_{\text{water}}t_1) \tag{8a}$$

$$S_3(t_1) = 3\sin(\Omega_{\text{water}}t_1) - \sin(3\Omega_{\text{water}}t_1) \tag{8b}$$

$S_2(t_1)$ and $S_3(t_1)$ reflect the intensity of intermolecular 2Q- and 3Q-derived residual water magnetization, respectively, as a function of t_1. The Fourier transform (FT) of eq 8a yields peak maxima at $(-2, 0, +2)^*(\Omega_{\text{water}}/2\pi)$ Hz in a 1:1:1 intensity ratio, and the FT of eq 8b, peak maxima at $(-3, -1, +1, +3)^*(\Omega_{\text{water}}/2\pi)$ Hz in a 1:3:3:1 intensity ratio. Note that the t_1 modulation frequencies indicated by eq 8 do not correspond directly to the evolution of the gradient-selected *n*Q coherences but rather reflect the evolution of the quantum states, created by the initial $90°_x$ pulse in Figure 1, which are subsequently transformed into the relevant *n*Q coherences by the second $90°_x$ pulse. The relative peak frequencies and intensities predicted by eqs 8a and 8b are in semiquantitative agreement with the experimental data presented in Figure 3 (parts C and D, respectively). A close examination of the t_1 profile data in Figure 3 reveals that when $\Omega_{\text{water}}t_1$ is an even multiple of π, a good null in the signal intensity of the residual water is obtained. In contrast, when $\Omega_{\text{water}}t_1$ is an odd multiple of π, only a minimum in intensity is obtained, but not a good null. This observation, in addition to the many other weak harmonics present in the F_1 frequency profiles in Figure 3, is not accounted for with the simple model described by eqs 7 and 8.

The explanation for these weak additional harmonic peaks may lie partly in a more thorough analysis of the basic assumptions inherent in eq 7: intermolecular *n*Q coherences arise solely from *n*-spin terms in σ^o, and radiation damping is ignored. For the pulse sequence depicted in Figure 1, values of $\Omega_{\text{water}}t_1$ that are odd multiples of π result in the water magnetization being placed along the $-z$ axis by the second 90° pulse. Radiation damping may then act to rotate the inverted water magnetization back to the +z axis. In contrast, values of $\Omega_{\text{water}}t_1$ that are even multiples of π result in the water magnetization being placed along the +z axis by the second 90° pulse. Magnetization along the +z axis is insensitive to the effects of radiation damping. Since the amount of water magnetization placed along the $-z$ axis depends upon t_1, the extent to which radiation damping acts to restore that magnetization to the +z axis must also depend upon t_1. It is in this way that radiation damping may act to modulate the signal intensity of residual water in t_1, thereby contributing to the additional resonance frequencies observed in Figure 3 (parts C and D).

Intermolecular *n*Q coherences can also arise from any *m*-spin term in σ^o where $m \geq n$. For example, the three-spin σ^o term $I_{z1}I_{z2}I_{z3}$ can give rise to the term $I_{z1}(I_2^+I_3^+ + I_2^-I_3^-)$ during Δ_2 (see Figure 1), which can subsequently lead to terms such as $I_{1y}I_{2z}I_{3z}$ at $t_2 = 0$. The latter term is finally refocused to observable I_{1y} magnetization during t_2 by dipolar coupling. The additional *m*-spin pathways leading to intermolecular water−water *n*Q coherences exhibit a t_1-dependence given by

$$\sin^{m-k}(\Omega_{\text{water}}t_1)\cos^k(\Omega_{\text{water}}t_1) \tag{9a}$$

where

$$k = (m - n) \text{ modulo } 2 \tag{9b}$$

and a θ dependence given by $[P_2(\cos\theta)]^{m-1}$. Furthermore, the actual intensity of the residual water signal that arises from such pathways also depends upon both the maximum value of the t_2 acquisition time and the recycle time. Finally, we conclude that the experimental data are consistent with the theory that intermolecular water−water *n*Q coherences arise from *m*-spin terms in σ^o where $m \geq n$.

If the intermolecular *n*Q-derived residual water magnetization in fact arises from higher order *m*-spin terms in σ^o, one would expect the intensity of this magnetization to become increasingly more sensitive to T_1 saturation effects for larger values of *m*. To test this expectation, we have measured the intensities of intermolecular 2Q- and 3Q-derived residual water magnetization in a sample of unlabeled BPTI in 90% water at $\theta = 0°$ for two different relaxation delays (RD): 2 and 25 s. The measured signal intensity is denoted as M_n(RD) where *n* represents the quantum order of the intermolecular water−water coherence. To simplify the analysis, t_1 has been set to $\pi/(2^*\Omega_{\text{water}})$. Only *n*Q pathways for which $k = 0$ (see eq 9) therefore contribute to the residual water magnetization observed during t_2. Furthermore, the single pathway with $n = m$ should dominate, as demonstrated by the results in Figure 3. The experimental results are summarized in Table 1 as $M_n(2)/M_n(25)$.

Since the pulse sequence in Figure 1 uses RF purge pulses to scramble all magnetization prior to the relaxation delay, the experimental recycle time T_{RC} is equivalent to RD. At least to a first approximation, one would heuristically expect the ratio of steady-state equilibrium magnetization (M_{nz}) to thermal equilibrium magnetization (M_{nz}^o) for an *n*-spin term in σ^o to be given by $(M_{nz}/M_{nz}^o)^n$. Incorporating these heuristic expectations into the standard equation describing T_1 saturation recovery, one obtains

$$M_{nz} \approx M_{nz}^o\{1 - \exp(-T_{\text{RC}}/_{T1})\}^n \tag{10}$$

The T_1 of the bulk water in this sample has been measured by saturation recovery to be 3.64 ± 0.01 s. Using $T_1(\text{water}) = 3.64$ s, we have calculated theoretical values for $M_n(2)/M_n(25)$ from eq 10 and present these values in Table 1. A comparison between the experimental and theoretical $M_2(2)/M_2(25)$ and $M_3(2)/M_3(25)$ values in Table 1 reveals reasonably good agreement. Thus, the intensities of the intermolecular water−water 2Q and 3Q coherences observed by this experiment scale quantitatively with the intensities of the two- and three-spin states in the

Table 1. Experimental and Calculated Ratios of Signal Intensities at Two Different Values of the Relaxation Delay for Intermolecular Water−Water *n*Q Coherences

	exptl (E)	calc (C)[a]
$M_2(2)/M_2(25)$	0.16	0.179
$M_3(2)/M_3(25)$	0.06	0.076

[a] Calculated using an experimental T_1(water) = 3.64 ± 0.01 s.

equilibrium density matrix, respectively. This observation strongly supports the interpretation that intermolecular *n*Q-derived residual water magnetizaton derives from these *n*-spin terms in σ^o. Based on eq 10, one also predicts that for normal recycle times used in NMR experiments applied to biological macromolecules ($T_{RC} \sim 1.2$ s), a dramatic decrease in the intensity of intermolecular water−water *n*Q coherences will occur as *n*, the coherence order, increases.

2QF-COSY

Figure 4 presents GE 2QF-COSY spectra on a 2 mM sample of unlabeled BPTI in 90% water. No presaturation of the water resonance during data acquisition and no low-frequency solvent filtration[18] during data processing have been employed. A limited two-step phasecycle ($\varphi_1 = x,-x$ and $\varphi_r = x,-x$) has been used. The data are presented in a phase-sensitive manner with F_1 quadrature by the hypercomplex method.[19] Gradients have not been used to obtain F_1 quadrature in these spectra. All gradients have the same θ value within a given experiment. Three cases have been examined: $\theta = 0°$ (Figure 4A; *z*-gradient); $\theta = 54.7°$ (Figure 4B; magic-angle-gradient); and $\theta = 90°$ (Figure 4C; *x*-gradient). The phase of the second 90° pulse is shifted 45° relative to that of the first 90° pulse ($\varphi_1 = 45°$).[20] In this way, the magnitude of the intermolecular water−water 2Q coherence is the same for both the real and imaginary parts of the complex t_1 interferogram. If these two 90° pulses have the same phase for the real t_1 component yet are 90° out-of-phase for the imaginary t_1 component, the intensity of the intermolecular water−water 2Q coherence will be much stronger in the F_2 spectrum comprising the imaginary t_1 component. The resulting differential baseline distortion between the two sets of F_2 spectra can lead to an F_1 quadrature artifact. The 45° phase shift largely eliminates this problem.

The residual water line along F_1 in the *z*-gradient 2QF-COSY spectrum (Figure 4A) is both wide and noisy, obscuring approximately 0.6 ppm in F_2 (4.35−4.95 ppm). There is also moderate "F_2-bleed", which manifests itself as streaks emanating from the F_1 water line that are parallel to the F_2 axis. In contrast, the residual water line is extremely narrow in the magic-angle 2QF-COSY spectrum (Figure 4B). The reduction in the intensity of the residual water signal by the magic-angle character of the gradients also leads to dramatically less F_2-bleed. Because F_2-bleed tends to arise from a lack of phase constancy in the detected residual water signal, the smaller the residual water signal, the smaller the magnitude of the F_2-bleed. Only a region of approximately 0.05 ppm in F_2 remains obscured by the residual water line in the magic-angle spectrum. This is a 12-fold improvement over the *z*-gradient spectrum and allows the identification of 13 additional $^1H_\alpha-^1H$ scalar correlations in BPTI. We have also acquired a *x*-gradient 2QF-COSY spectrum (Figure 4C), in which the residual water line obscures approximately 0.3 ppm in F_2 (4.5−4.8 ppm). Although the obscured region is two-fold more narrow than that in the *z*-gradient spectrum, it is nonetheless six-fold wider than that in the magic-angle spectrum. Compared to the *z*-gradient spectrum, the *x*-gradient spectrum allows the identification of seven additional $^1H_\alpha-^1H$ scalar correlations in BPTI. Practically, *x*-gradients yield better water suppression than *z*-gradients in the GE 2QF-COSY, but magic-angle gradients are superior to either *z*- or *x*-gradients in this regard.

We have also examined the effect of the limited phase cycling on the residual water intensity. Because a major source of residual water signal in the GE 2QF-COSY experiment is expected to arise from two-spin terms in σ^o that exist at the end of the relaxation delay, one would predict that cycling the phase φ_1 of the first 90° pulse ($x,-x$) in concert with the receiver phase φ_r should further attenuate that signal. 1D 2Q-filtered experiments have confirmed this prediction, demonstrating a 5-fold reduction in water signal intensity upon implementation of this two-step phasecycle. These data are shown in Figure 5 (parts A and B). Consistent with the theory, we have also observed a minimal reduction in the intensity of the residual water signal in 1D 3Q-filtered experiments following the implementation of the same two-step phase cycle. These data are shown in Figures 5 (parts C and D).

Van Zijl and co-workers have recently published similar results for a GE 2QF-COSY experiment in which magic-angle gradients were employed.[13] Their experiment, however, used more extensive phase cycling and did not remove the effects of radiation damping during t_1 on ^1H resonances (usually $^1H_\alpha$) that lie sufficiently close to the water resonance. Furthermore, the magic-angle character of their gradient pulses was achieved through the simultaneous application of three equistrength orthogonal gradients. In theory, a minimum of two orthogonal gradient coils is necessary to generate a magic-angle gradient. In practice, we have shown in Figure 4 that magic-angle gradients generated with only two orthogonal gradient coils are sufficient to obtain significant gains in water suppression in GE 2QF-COSY spectra.

NH-HSQC and CC-NOESY

We have also investigated the benefit of magic-angle gradients in the gradient-enhanced, sensitivity-enhanced $^1H-^{15}N$ HSQC[21] (GESE-HSQC) with water-flipback pulses.[22] One observes that because such sequences preserve single-spin water magnetization (I_z terms in σ^o) throughout the course of the RF pulse train, they should also preserve *n*-spin water−water states. For this reason, water−water MQ coherences will not be efficiently excited during the pulse sequence, and magic-angle gradients may provide only a minimal improvement in overall water suppression in this type of experiment. Two separate $^1H-^{15}N$ GESE-HSQC spectra have been acquired on a 1 mM sample of $^{13}C/^{15}N$-labeled ubiquitin: one with $\theta = 0°$ and the other with $\theta = 54.7°$ for all gradients. These data are provided in the supporting information (Figure 9). No presaturation of the water resonance during acquisition and no low-frequency solvent filtration during data processing have been employed. A comparison of the level and quality of water suppression between these two HSQC spectra reveals no readily discernible differences.

(18) Marion, D.; Bax, A. *J. Magn. Reson.* **1989**, *83*, 205−211.
(19) States, D. J.; Haberkorn, R. A.; Ruben, D. J. *J. Magn. Reson.* **1982**, *48*, 286−292.
(20) Stonehouse, J.; Clowes, R. T.; Shaw, G. L.; Keeler, J.; Laue, E. D. *J. Biomol. NMR* **1995**, *5*, 226−232.
(21) Kay, L. E.; Keifer, P.; Saarinen, T. *J. Am. Chem. Soc.* **1992**, *114*, 10663−10665.
(22) Grzesiek, S.; Bax, A. *J. Am. Chem. Soc.* **1993**, *115*, 12593−12594.

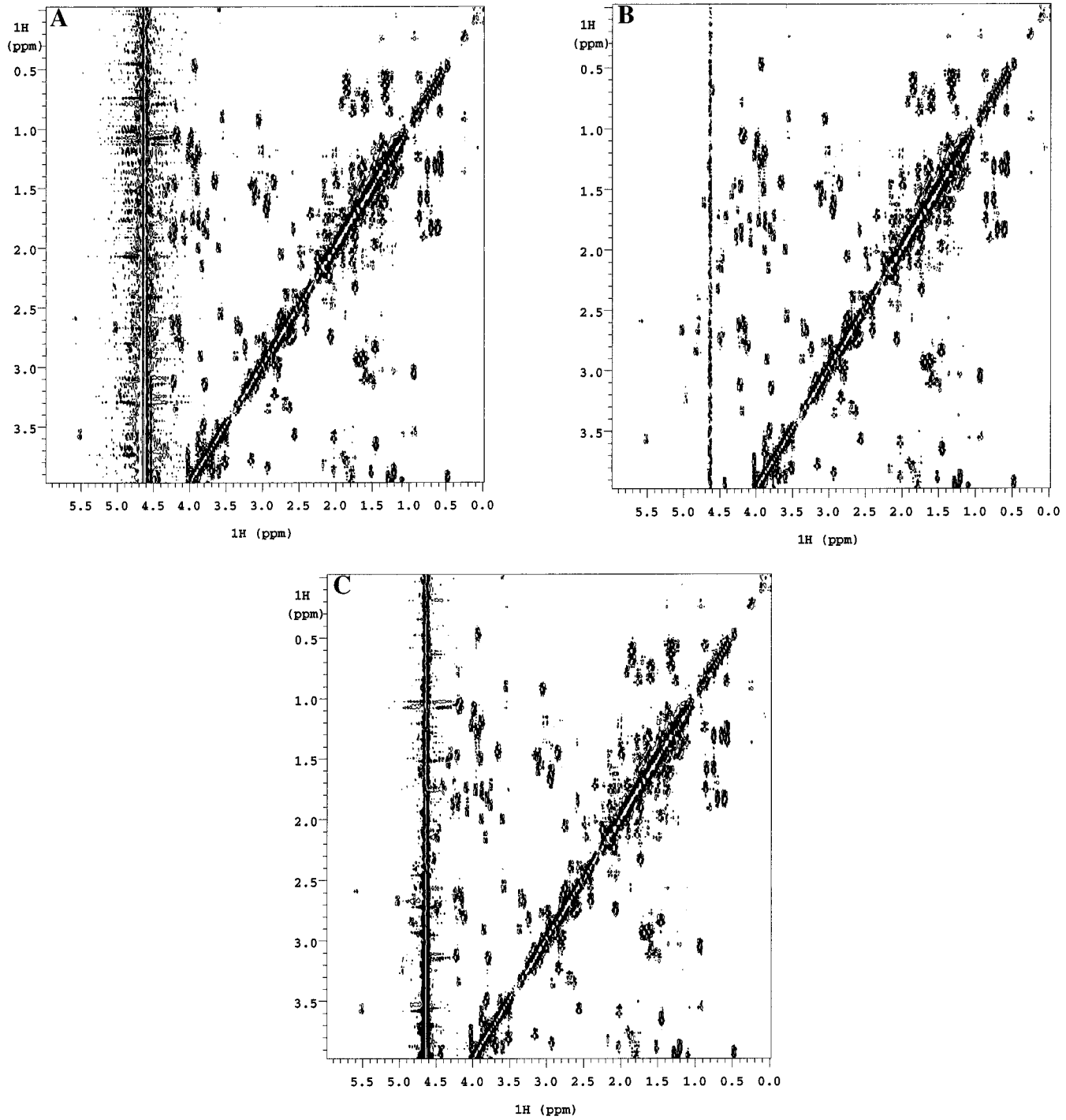

Figure 4. 2D ^{1}H$-^1$H GE 2QF-COSY spectra recorded on a sample of 2 mM unlabeled BPTI in 90% water. The pulse sequence of Figure 1 was used with all gradients having the same angles (θ, ϕ) within a given experiment. ϕ was fixed at 0°. Acquisition parameters were sw(F_1) = 10 kHz, t_1^{max} = 25.5 ms, Δ_1 = 0.4 ms, Δ_2 = 1.1 ms, G_1 = 7.9 G/cm for 0.3 ms, G_2 = 7.9 G/cm for 1 ms, G_3 = 15.8 G/cm for 1 ms, G_4 = 14.8 G/cm for 10 ms, SL_x = 4.0 ms, SL_y = 2.5 ms, and $\gamma B_1(^1H_{SL}) \sim$ 18.5 kHz. The phase cycle was $\varphi_1 = x, -x$; $\varphi_2 = 45°$; and $\varphi_r = x, -x$. Four transients were signal-averaged per FID. The data were collected at 30.0 °C on a Varian UnityPlus 600 using a ^{1}H/^{13}C/^{15}N triple-resonance probe equipped with a self-shielded triple-axis gradient coil. All gradients were rectangular in shape. No passive eddy current compensation or gradient-amplifier blanking was used: (A) $\theta = 0°$, (B) $\theta = 54.7°$, and (C) $\theta = 90°$.

A similar comparison has also been made for the 4D gradient-enhanced, constant-time, coherence-transfer-echo ^{13}C/^{13}C-separated NOESY[23] (Figure 10 in supporting information). There are at least two reasons why this particular ^{13}C/^{13}C-separated NOESY should benefit more from magic-angle gradients than the ^{1}H$-^{15}$N GESE-HSQC with regards to water suppression. Firstly, it has not been possible in this NOESY both to preserve water magnetization and to maintain a sufficient level of gradient-based artifact suppression. Secondly, gradients are used to select the $^{13}C_{acceptor}$ sinqle-quantum coherence during the constant-time t_3 evolution period. This is analogous to the gradient-based coherence selection performed in the previous GE nQF-COSY experiments. Two separate 2D ^{13}C/^{13}C-filtered NOESY spectra have been acquired on a 1 mM sample of ^{13}C/^{15}N-labeled ubiquitin: one with $\theta = 0°$ (Figure 6A) and the other with $\theta = 54.7°$ (Figure 6B) for all gradients. Only two

(23) Farmer II, B. T.; Metzler, W. J.; Mueller, L. Manuscript in preparation.

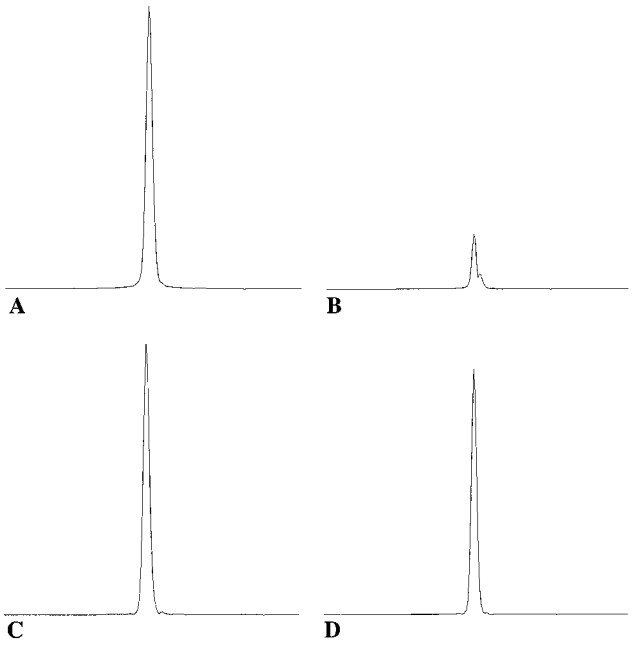

Figure 5. These data were collected on the same sample and with the same pulse sequence as described in the legend to Figure 4. Two transients were signal-averaged per FID. The water signal was placed 500 Hz off resonance; and t_1 was set to 0.5 ms: (A, B) 2Q-filtered residual water magnetization for $\varphi_1 = \varphi_r = (x, x)$ and $\varphi_1 = \varphi_r = (x, -x)$, respectively and (C, D) 3Q-filtered residual water magnetization for $\varphi_1 = \varphi_r = (x, x)$ and $\varphi_1 = \varphi_r = (x, -x)$, respectively.

transients are signal-averaged per FID. The phase of the $^{13}C_{don}$ 90° sampling pulse is cycled $(x,-x)$ in concert with the receiver phase. A comparison of these two $^{13}C/^{13}C$-filtered NOESY spectra reveals that better water suppression and less "F_4-bleed" are afforded by magic-angle gradients than by *z*-gradients. Unfortunately, the level of improvement in the NOESY is not as dramatic as that observed in the 2QF-COSY spectra (Figure 4). There are at least two factors, however, that determine the overall level of water suppression in any heteronuclear-filtered experiment: (1) the level of water suppression per transient and (2) the level of signal cancellation that can be achieved by cycling the receiver phase $(x,-x)$. 1D first increments from the $^{13}C/^{13}C$-filtered NOESY, presented in Figure 7, indicate that the level of water suppression *per transient* is significantly better with magic-angle gradients than with *z*-gradients but that the final level of water suppression after two transients is only moderately better. The explanation for the latter observation is currently unknown.

Discussion

All of the experimental evidence presented in this study strongly supports key aspects of the theory, originally proposed by Warren *et al.*,[2] to explain intermolecular solute−water and water−water MQ coherences. The (θ, ϕ)-profile data in Figure 2 are consistent with the theory that intermolecular water−water single-quantum coherences are refocused to observable magnetization during t_2 by a macroscopic dipolar effect. Both the t_1- and F_1-profile data in Figure 3 and the T_1 relaxation data support the contention that the origin of these MQ coherences lies in higher-order terms in σ^o.

The incorporation of a dipolar demagnetizing field into the Bloch equations has also been used to explain the origin of these MQ coherences.[1,8] Two studies relate these additional peaks to the phenomenon of multiple echoes in concentrated solutions,

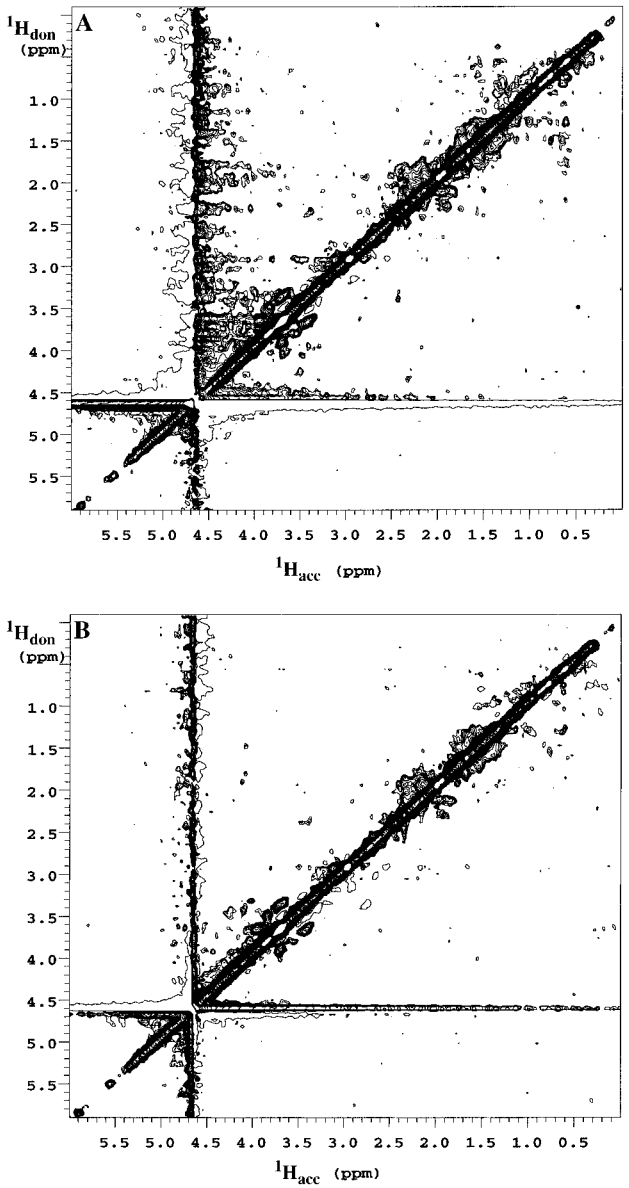

Figure 6. 2D $^{13}C/^{13}C$-filtered NOESY spectra recorded on a 1 mM sample of $^{13}C/^{15}N$-labeled ubiquitin using the 4D $^{13}C/^{13}C$-separated, constant-time, coherence-transfer-echo NOESY pulse sequence.[23] A diagram of the pulse sequence and relevant acquisition parameters are provided as supporting information (Figure 10). All gradients have the same angles (θ, ϕ) within a given experiment. ϕ was fixed at 0°. No water-flipback pulses[22] were employed. Gradient-based coherence selection[30,31] was used to achieve ^{13}C editing in the $^1H_{acceptor}$ dimension. The mixing time was set to 100 ms. Two transients were signal-averaged per FID. The data were collected at 30.0 °C on a Varian UnityPlus 500 using a $^1H/^{13}C/^{15}N$ triple-resonance probe equipped with a self-shielded triple-axis gradient coil. All gradients were rectangular in shape. No passive eddy current compensation or gradient-amplifier blanking was used: (A) $\theta = 0°$ and (B) $\theta = 54.7°$.

first explored in ^3He[24,25] and recently in more conventional samples such as pure water.[11,12,26] In both of these studies, the classical Bloch equations have been modified as previously described[24] to include the "dipolar demagnetizing field". This theoretical treatment yields good agreement with experiment for simple pulse sequences. Warren and co-workers have

(24) Deville, G.; Bernier, M.; Delrieux, J. M. *Phys. Rev. B* **1979**, *19*, 5666−5688.
(25) Einzel, D.; Eska, G.; Hirayoshi, Y.; Kopp, T.; Wölfle, P. *Phys. Rev. Lett.* **1984**, *53*, 2312−2315.
(26) Bedford, A. S.; Bowtell, R.; Bowley, R. M. *J. Magn. Reson.* **1991**, *93*, 516−532.

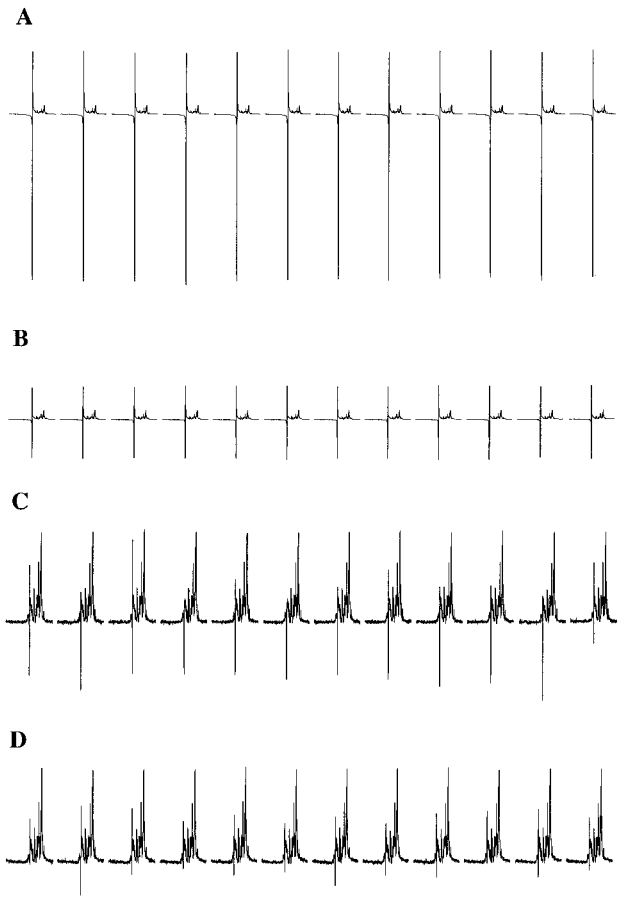

Figure 7. 1D first increments from the $^{13}C/^{13}C$-filtered NOESY. The effect of θ and nt (number of transients per FID) on the magnitude of the residual water signal is illustrated. Only the phase of the $^{13}C_{don}$ 90° pulse is cycled (x, $-x$) in concert with the receiver phase φ_r for nt = 2. Spectra acquired with the same number of transients are plotted at the same vertical scale: (A) $\theta = 0°$ and nt = 1, (B) $\theta = 54.7°$ and nt = 1, (C) $\theta = 0°$ and nt = 2, and (D) $\theta = 54.7°$ and nt = 2.

recently shown that a corrected version of the demagnetizing-field treatment and the quantum (density-matrix) treatment give exactly the same answer under certain assumptions that are usually met in liquids.[10,27] Even though the classical and quantum models give the same answer in principle, they have different strengths in practice: the classical model is usually much less intuitive and provides less predictive power than the quantum model used in this paper, but the former is often better for including effects such as radiation damping and diffusion.

The data presented in Figure 2 clearly indicate that the intensity of magnetization arising from intermolecular water−water 2Q coherence is the most sensitive to deviations from the magic-angle in the gradient pulses. Higher-order coherences are much more forgiving due to the exponential nature of the $P_2(\cos\theta)$ dependence. In addition, the GE 2QF-COSY results on BPTI in Figure 4 demonstrate that magic-angle gradients generated with only two orthogonal gradient coils suffice in a practical sense. These observations suggest that a single-axis gradient coil whose gradient direction is either at or close to the magic angle should be sufficient to realize the improvements in water suppression described in this report. Moreover, the design of such a gradient coil has already been proposed and evaluated at 500 MHz on a 5mm sample of water.[28] For 8 mm probes, a single-axis, magic-angle gradient coil may provide the needed improvement in overall water suppression without incurring any additional degradation in RF performance.

The extension of magic-angle gradients to heteronuclear double-resonance experiments has not yet yielded a dramatic improvement in water suppression. There are perhaps several reasons for this. First, a typical recycle time for these experiments is 1.2 s. The maximum intensity for an intermolecular water−water nQ coherence is therefore reduced by $(0.281)^n$ relative to that obtained with a recycle time > 20 s. Second, techniques which minimize the amount of transverse water magnetization at the end of the RF pulse train are becoming more widespread in ^1H_N-based/detected double- and triple-resonance experiments.[20,22,32] These techniques, however, also tend to minimize the excitation of intermolecular water−water nQ coherences from higher-order terms in σ^o. Nonetheless, magic-angle gradients have yielded dramatic increases in the level of water suppression in GE nQF-COSY spectra, both in our laboratories and in others,[13] and have also provided the means to validate a novel theory[2] describing the creation/detection of intermolecular MQ coherences.

Acknowledgment. W.S.W is supported by the NIH under contract GM35253. D.M. acknowledges Prof. Gaetano Montelione of Rutgers University for providing a sample in the early stages of this work. D.M. and B.T.F. thank Layne Howard, Bill Llanos, and Mike Cummings of Varian Associates for their assistance with the triple-resonance, triple-axis gradient probe.

Supporting Information Available: Spectra of 2Q-filtered residual water magnetization as a function of θ; ^1H-^{15}N GESE-HSQC spectra on $^{13}C/^{15}N$-labeled ubiquitin for $\theta = 0°$ and $\theta = 54.7°$; pulse sequence and parameters for the 4D $^{13}C/^{13}C$-filtered NOESY (6 pages). This material is contained in many libraries on microfiche, immediately follows this article in the microfilm version of the journal, can be ordered from the ACS, and can be downloaded from the Internet; see any current masthead page for ordering information and Internet access instructions.

JA953186O

(27) Lee, S.; Richter, W.; Vathyam, S.; Warren, W. S. *J. Chem. Phys.*, in press.

(28) Bowtell, R.; Peters, A. *J. Magn. Reson. Ser. A* **1995**, *115*, 55−59.

(29) Messerle, B. A.; Wider, G.; Otting, G.; Weber, C.; Wuthrich, K. *J. Magn. Reson.* **1989**, *85*, 608−613.

(30) Boyd, J.; Soffe, N.; John, B. K.; Plant, D.; Hurd, R. *J. Magn. Reson.* **1992**, *98*, 660−664.

(31) Ruiz-Cabello, J.; Vuister, G. W.; Moonen, C. T. W.; van Gelderen, P.; Cohen, J. S.; van Zijl, P. C. M. *J. Magn. Reson.* **1992**, *100*, 282−302.

(32) Kay, L. E.; Xu, G. Y.; Yamazaki, T. *J. Magn. Reson. Ser. A* **1994**, *109*, 129−134. Kuboniwa, H.; Grzesiek, S.; Delaglio, F.; Bax, A. *J. Biomol. NMR* **1994**, *4*, 871−878. Yamazaki, T.; Pascal, S. M.; Singer, A. U.; Forman-Kay, J. D.; Kay, L. E. *J. Am. Chem. Soc.* **1995**, *117*, 3556−3564. Farmer, B. T., II; Venters, R. A. *J. Biomol. NMR*, in press.